THE ASTRONOMICAL JOURNAL, 119:1325–1338, 2000 March

THE NATURE OF THE *IRAS* RING G159.6−18.5 IN PERSEUS AND ITS EXCITING STAR HD 278942

B-G ANDERSSON[1,2]
Center for Astrophysical Sciences, Johns Hopkins University, 3400 North Charles Street, Baltimore, MD 21218; bg@pha.jhu.edu
P. G. WANNIER[1]
Jet Propulsion Laboratory, California Institute of Technology, 4800 Oak Grove Drive, Pasadena, CA 91109; peter.wannier@jpl.nasa.gov
G. H. MORIARTY-SCHIEVEN[3,4]
National Research Council of Canada and Joint Astronomy Centre, 660 North A'ohōkū Place, Hilo, HI 96720; gms@jach.hawaii.edu
AND
E. J. BAKKER[1,5]
Department of Astronomy, University of Texas, Austin, TX 78712; e.j.bakker@fel.tno.nl
Received 1999 September 1; accepted 1999 November 18

ABSTRACT

We discuss an extended feature in the Perseus molecular cloud complex, which is most prominent in the *IRAS* database as an almost complete ring of radius 0.°75 but is also clearly seen in optical surveys and in radio continuum emission. While earlier identified as a supernova remnant, we argue that the feature is probably an H II region, based on new interferometric radio continuum data at 408 and 1420 MHz, diffuse Hα emission, and the identification of HD 278942 as an O9.5–B0 V star located at the geometric center of the *IRAS* ring. The spectral index of the radio continuum emission is consistent with an optically thin H II region. However, an origin of the radio continuum emission as at least partially caused by synchrotron emission from the interaction region between the stellar wind and the remaining molecular cloud cannot be ruled out. We present visual photometry, spectroscopy, and polarimetry of the star HD 278942, which we believe to be the source of the excitation for the H II region and the stellar wind. While coincident with an *IRAS* point source, no compact radio continuum source is seen at the location of the star. Null results for CO $J = 1$–0 emission different from the ambient cloud are reported. The possibility that HD 278942 is a main-sequence star with a circumstellar disk is suggested.

Key words: H II regions — ISM: individual (Perseus molecular cloud, G159.6−18.5) — stars: formation

1. INTRODUCTION

An almost complete ring of enhanced emission can be seen in the *IRAS* 100 μm data toward the Perseus molecular cloud complex (Fig. 1). This was first described by Pauls & Schwartz (1989) and further discussed by Fiedler et al. (1994). These authors argue, based on radio data, that the feature is caused by a supernova remnant (SNR), which would in such a case have the highest known galactic latitude. Recently, de Zeeuw et al. (1999) have associated the *IRAS* ring with the star HD 278942 (=AG +31°346 = HIP 17113). Here we expand on this identification and analyze several new data sets that have bearing on the star-cloud interaction.

The Perseus molecular cloud complex has a mass of about $1.3 \times 10^4\ M_\odot$ at a distance of 260 pc (Cernicharo, Bachiller, & Duvert 1985; Černis 1993). A generally ordered magnetic field permeates the cloud complex and runs along its major axis, as can be deduced from optical polarimetry of background stars (Goodman et al. 1990; Wannier & Andersson 1996). Goodman et al. (1989) used Zeeman splitting measurements in the OH λ doublet transitions at 1665 and 1667 MHz to derive a line-of-sight component of the magnetic field of -27 ± 4 μG. Since the cloud geometry and optical polarimetry indicate that the magnetic field is probably oriented close to the plane of the sky, the true magnetic field strength is likely significantly in excess of this value. Star formation is taking place in several parts of the complex, most obviously around the two reflection nebulae IC 348 and NGC 1333. However, Ladd, Lada, & Meyers (1992) surveyed the entire complex for 2 μm sources and found pre–main-sequence sources throughout the cloud. The regions of intense star formation, IC 348 and NGC 1333, have been observed, respectively, at near-infrared wavelengths by Lada & Lada (1995) and Aspin, Sandell, & Russell (1994) and at X-ray wavelengths by Preibisch, Zinnecker, & Harbig (1996) and Preibisch (1997). A large number of pre–main-sequence and main-sequence stars have been detected by these surveys. However, relatively few high-mass stars have been found in these young clusters. The interaction of newly formed stars with the parent cloud, particularly in the case of massive stars, can have significant consequences for the subsequent development of the cloud. Hot, massive stars cause cloud disruption through their ionizing flux as well as through the momentum in their stellar winds. On the other hand, given the right conditions in the cloud, their stellar winds can also cause the collapse of cloud cores and induce further star formation (Foster & Boss 1996). Hence, the development of an embedded O/B star is an important chapter in the star formation history of the Perseus complex.

2. OBSERVATIONS AND DATA REDUCTION

This paper is based on a range of observations, including radio, millimeter-wave, infrared, and optical. Most of the

[1] Visiting Astronomer, McDonald Observatory, University of Texas, Austin.
[2] Guest Observer, Table Mountain Observatory, Jet Propulsion Laboratory.
[3] Guest Observer, National Radio Astronomy Observatory.
[4] Guest Observer, James Clark Maxwell Telescope.
[5] Current address: TNO-FEL Electro Optics Group, P.O. Box 96864, 2509 JG, The Hague, Netherlands.

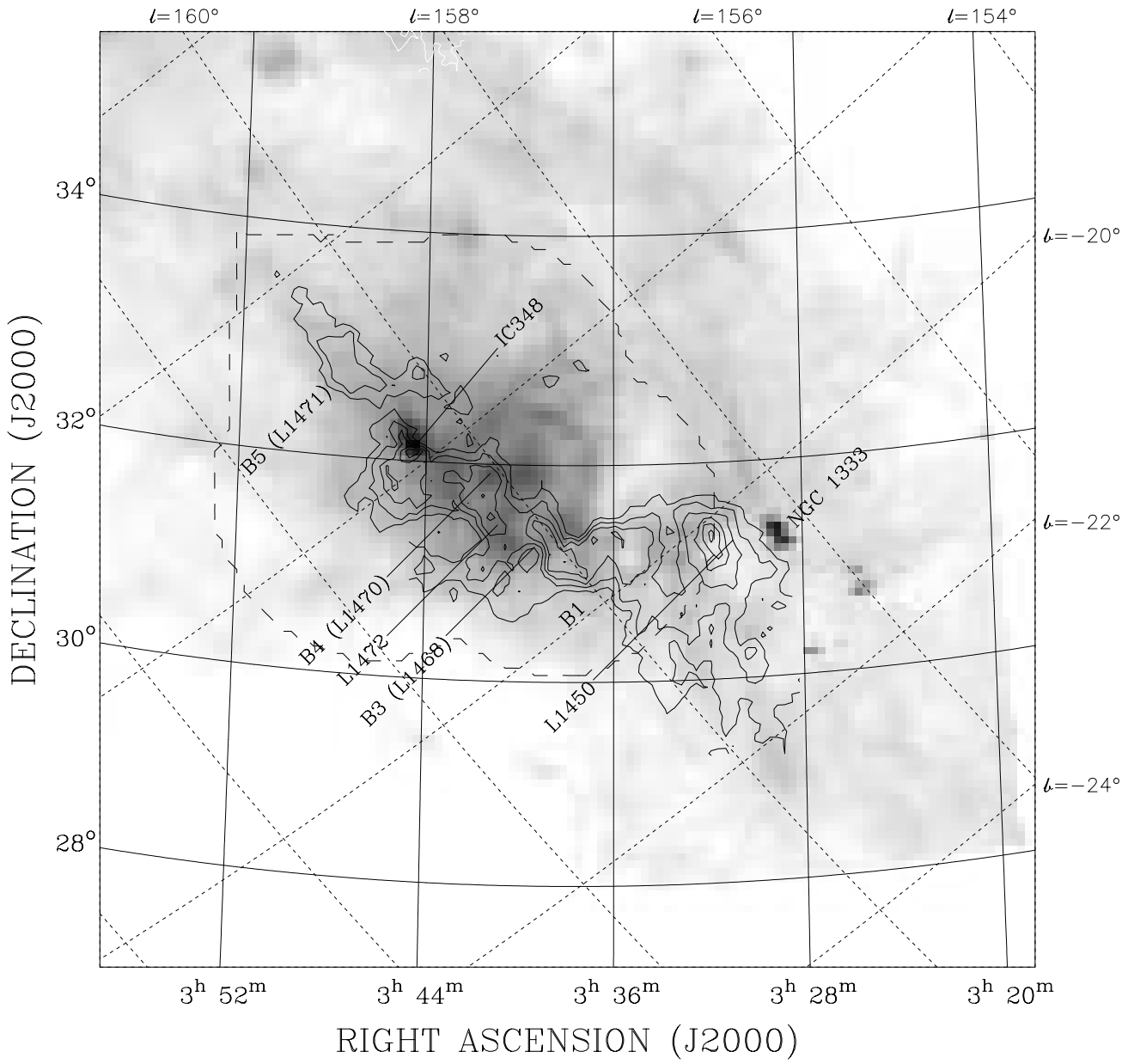

FIG. 1.—Gray-scale map of the 100 μm emission and a contour map of CO emission in the Perseus molecular cloud provide a "road map" to the *IRAS* ring feature discussed in this paper. The ring is the prominent feature centered at about 3^h40^m, $+32°$. We have noted the main features of the complex, including the main subclouds as well as the two open clusters, IC 348 and NGC 1333. The dashed curve illustrates the approximate extent of the 1420 MHz continuum map discussed in this study.

observations are presented elsewhere, so we discuss in detail only those not covered in other papers. We have also made use of data in the public domain, such as POSS-II and star-count data by Cernicharo & Bachiller (1984).

2.1. *Radio Observations*

The radio continuum observations were acquired with the synthesis telescope (ST) at the Dominion Radio Astrophysical Observatory[6] (DRAO), Penticton, Canada, during 1994 January and March. The observing and data reduction are discussed in detail by Wannier et al. (2000), with the differences that single-dish, low-order spacing data (i.e., baselines less than 12 m) were not added to the continuum maps and that the continuum maps were cleaned and self-calibrated before being combined into a mosaic. For the present purpose, we note that the ST samples almost the entire *u-v* plane (from 12 to 600 m) and, hence, is sensitive to small spatial scales down to the resolution of the array ($\sim 6\farcm5 \times 3\farcm3$ for the 408 MHz map and $\sim 3\farcm75 \times 2'$ for the 1420 MHz map with the position angle of the major axis oriented north-south). However, because of the missing short spacings, the flux from diffuse emission could potentially be underestimated. The data have (1 σ) sensitivity

[6] The Dominion Radio Astrophysical Observatory is operated as a national facility by the Herzberg Institute for Astrophysics of the National Research Council of Canada.

limits of 3.3 mJy beam^{-1} (408 MHz) and 0.23 mJy beam^{-1} (1420 MHz) at the map center.

2.2. *Millimeter-wave Observations*

Observations of ^{12}CO $J = 2$–1 and ^{13}CO $J = 1$–0 were acquired with the NRAO[7] 12 m telescope on Kitt Peak, Arizona, during 1996 December 6–11. Dual polarization SIS receivers yielded system temperatures on the sky of about 250 K for ^{13}CO $J = 1$–0, and 750 K for ^{12}CO $J = 2$–1. A hybrid autocorrelator spectrometer was used with a maximum spectral resolution of 48 kHz. The data were taken in frequency-switching mode, switching by ± 2 to ± 4 MHz. We mapped a $1.'8 \times 1.'8$ region in ^{12}CO $J = 2$–1 plus a $2.'9 \times 2.'9$ region in ^{13}CO $J = 1$–0 centered on the location of HD 278942, as well as two cuts across the intensity enhancement in the north and west limbs of the *IRAS* ring. After folding the frequency-switched spectra and averaging the two polarizations, the typical $\sigma_{\rm rms}$ per channel was 0.4 and 0.1 K for ^{12}CO $J = 2$–1 and ^{13}CO $J = 1$–0, respectively.

2.3. *850 μm Continuum Observation*

Submillimeter-wave photometry was acquired at the James Clark Maxwell Telescope (JMCT)[8] on Mauna Kea, Hawaii, on 1997 August 22. We used the SCUBA array in photometry mode, following a standard observing procedure in which the source is averaged over an area somewhat larger than the primary beam by jiggling in a nine-point pattern while simultaneously chopping the secondary mirror (Ivison et al. 1998). At 850 μm, JCMT has a beamwidth of $14.''5$; for these observations, a chop throw of $60''$ was used. We did not detect any point source associated with HD 278942. After a total integration time of 48 minutes, a 3 σ upper limit of 7.3 mJy was achieved.

2.4. *IRAS Data*

IRAS data were extracted in the FRESCO mode from the *IRAS* data base at IPAC.[9] This calibrated data product is co-added and de-striped and represents the full resolution, without any resolution-enhancement techniques or smoothing. We used the algorithms of Kuiper et al. (1987) to derive dust temperatures and optical depths based on the 60 and 100 μm bands. Since the 60–100 μm flux ratio is between 0.3 and 0.9, we use the approximations T_2 and N_2 (see Kuiper et al. 1987) as temperature and column density measures, with the modification that we use the more direct measure of dust opacity rather than assuming a gas-to-dust ratio and quoting the column density of the gas.

2.5. *Visual Wavelength Observations*

Photometry of HD 278942 was acquired at the Table Mountain Observatory during the night of 1995 November 28 using the $24''$ telescope and a Thompson 512×512 CCD, with a pixel size of $0.''5$ on the sky. The *B* and *V* filters of the Johnson system were used. Because of the low blue sensitivity of the CCD, the *U* filter was not used. Several (eight) HR catalog stars were used as standards, with care being taken to cover a variety of intrinsic colors as well as different air masses throughout the night. The data were reduced using the IRAF PHOTCAL package, after the standard CCD corrections (bias, dark, and flatfield) had been performed. Although the night was of only marginal photometric quality with average seeing of $\approx 3''$, the reduction, including sky correction, converged and produced satisfactory results.

Polarimetry measurements of HD 278942 were acquired with the photopolarimeter (Breger 1979) on the 82 inch (2.1 m) telescope at the McDonald Observatory during the nights of 1994 October 2–5. For HD 278942, measurements were made in the *B*, *V*, *R*, and *I* filters of the extended Johnson system using a single aperture of $14.''73$. The details of the observing and data reduction are discussed in Andersson & Wannier (1996).

Echelle spectra of HD 278942 were acquired with the 107 inch (2.7 m) telescope of the McDonald Observatory during the night of 1996 December 19, using the coudé spectrograph (Tull et al. 1995) and a Tektronix 2048×2048 CCD. The spectra covered wavelengths between 3820 and 10750 Å, with continuous coverage of the region 3850–5000 Å. Wavelength calibration was achieved by observing a Th-Ar hollow cathode lamp at several times during the observations. The spectral resolution was measured to be $R \approx 50{,}000$. Data reduction was performed with standard IRAF procedures, and the echelle orders were extracted into one-dimensional spectra. After normalization, the individual orders were combined to form a continuous one-dimensional spectrum, which was used for the stellar spectral classification. For detailed analysis, such as the C_2 measurements, smaller pieces of the spectrum were extracted.

3. RESULTS

3.1. *Radio Continuum Maps*

At both 408 and 1420 MHz, faint extended emission is seen inside the *IRAS* ring (Fig. 2). As always, a large number of radio continuum sources also can be seen in the maps. In Tables 1 and 2, we list the brightest sources within a few degrees of the star. For 408 MHz, sources with integrated intensities brighter than 0.3 Jy are listed, while for 1420 MHz, we chose a cutoff of 30 mJy. We provide these tables here as they may be useful as source lists for absorption-line studies of the cloud complex. A weak 21 cm continuum source (9.7 ± 0.6 mJy) is located $2.'4$ from the optical position of HD 278942. Given that the offsets between radio and optical coordinates are usually significantly smaller than this (e.g., Riley 1989), and given the large number of radio continuum sources in the field, we do not feel that this source can be reliably associated with the star. The extended emission, however, is associated with the *IRAS* ring, as can be seen from Figure 2, where, for clarity, we have overlaid the outline of the 100 μm ring as the dashed white curve.

We used a point source–subtracted map to derive the intensities for this emission, excluding a small region around the brightest 408 MHz source (No. 1), because of the imperfect subtraction of this source. An irregular polygon

[7] The National Radio Astronomy Observatory is a facility of the National Science Foundation, operated under cooperative agreement by Associated Universities, Inc.

[8] The JCMT is operated by the Royal Observatory of Edinburgh on behalf of the Particle Physics and Astronomy Research Council of the United Kingdom, the Netherlands Organization for Scientific Research, and the National Research Council of Canada.

[9] IPAC is funded by NASA as part of the extended *IRAS* mission under contract to JPL.

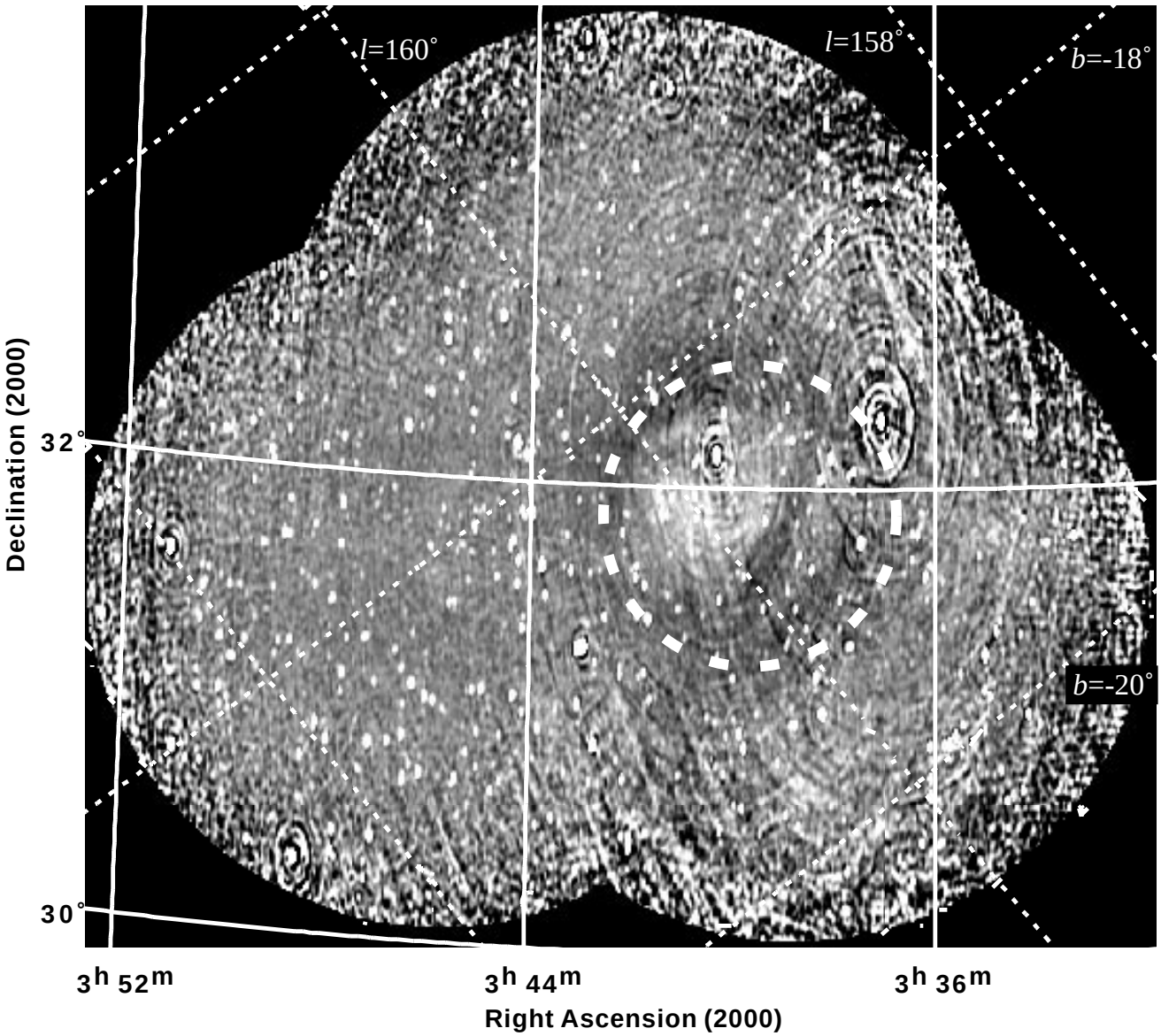

FIG. 2.—Mosaic of three ST fields of 1420 MHz continuum emission clearly showing the low-level diffuse emission caused by the H II region responsible for the *IRAS* ring. A large number of background radio sources also can be seen. Note, in particular, source 1 (see Table 1), which is located close to the diffuse emission. It is only after careful subtraction of these point sources that reliable fluxes can be integrated for the H II region.

was constructed in the images inside of which the flux was integrated. We find integrated fluxes of 2.0 Jy for the 408 MHz band and 1.4 Jy for the 1420 MHz band, with integration uncertainties of about 0.1 Jy in either band. Because no short spacings were included in the map synthesis, the uncertainties for these numbers are highly asymmetrical. We can estimate the amount of flux missing because of the incomplete sampling of the *u-v* plane based on interferometry theory (e.g., Fomalont 1989). If we assume a uniform source of $30'' \times 30''$ extent, we find that for 1420 MHz, up to about $\frac{3}{4}$ of the total flux may be missing, while for 408 MHz, only up to about $\frac{1}{4}$ of the flux should be missing. This then yields flux estimates of $F(408\ \mathrm{MHz}) = 2.0^{+0.8}_{-0.1}$ Jy and $F(1420\ \mathrm{MHz}) = 1.4^{+4.3}_{-0.1}$ Jy, which in turn yield a spectral index $[F(\nu) \propto \nu^{\alpha}]$ of $\alpha = -0.3^{+0.3}_{-1.1}$. This value is consistent with that for an optically thin H II region ($\alpha = 0$), albeit with large uncertainties. We suspect that, whereas we are influenced by missing short spacings, earlier studies (e.g., Fiedler et al. 1994) that have shown more negative spectral indices may have been misled by the inability to resolve the diffuse source from one or more of the discreet sources. In particular, our source 1 (= 3C92), with integrated fluxes at 408 and 1420 MHz of 4.5 and 1.4 Jy, respectively, and a spectral index of -0.93 could be a problem. We note, however, that Pauls (1999) using VLA D-array (327 MHz) and Effelsberg (2700 MHz) data find a spectral index of $\alpha = -0.9$.

3.2. CO *Maps*

The CO maps are dominated by the diffuse CO emission from the Perseus molecular cloud. Although some spatial variation occurs near HD 278942, none can be attributed clearly to the star or to possible circumstellar material (Fig. 3). Specifically, the spectra directly toward the star do not show any line wings at a level of 0.5 K in the ^{12}CO $J = 2$–1 data and 0.1 K in the ^{13}CO $J = 1$–0 data. Also, the cuts across the *IRAS* ring are dominated by ambient material

TABLE 1

408 MHz Sources

Source	R.A. (J2000)	Decl. (J2000)	Integrated Flux (mJy)	Peak Flux (mJy)	Size (arcsec)	P.A.[a] (deg)
5.....	3 34 17.01 ± 0.14	31 12 05.9 ± 2.7	677.5 ± 27.4	(677.8 ± 22.8)	...	...
11.....	3 35 04.52 ± 0.15	30 47 20.9 ± 2.4	421.5 ± 16.2	(375.8 ± 12.4)	...	...
3.....	3 36 29.91 ± 0.11	32 18 24.7 ± 1.4	2126.8 ± 67.2	(2127.5 ± 64.9)	...	...
4.....	3 36 59.29 ± 0.11	31 44 06.2 ± 1.4	896.4 ± 28.5	(896.8 ± 27.4)	...	...
16.....	3 37 43.72	32 06 23.8	488.7 (centroid)	...	...	...
16A.....	3 37 36.20 ± 0.61	32 07 44.5 ± 9.7	184.6 ± 23.1	(184.8 ± 11.3)	...	...
16B.....	3 37 51.16 ± 0.65	32 03 10.3 ± 20.2	220.7 ± 25.7	(146.4 ± 9.5)	6.9 × 0.8	2
13.....	3 37 50.49 ± 0.17	31 14 51.1 ± 3.5	353.3 ± 16.0	(322.4 ± 11.5)	...	...
7.....	3 37 51.44 ± 0.15	30 55 57.6 ± 3.0	673.8 ± 75.7	(674.0 ± 23.5)	...	...
1.....	3 40 08.28 ± 0.11	32 09 01.3 ± 1.3	4452.1 ± 139.2	(4454.2 ± 135.4)	...	...
6.....	3 42 54.40 ± 0.13	30 47 38.2 ± 2.2	683.4 ± 25.2	(683.9 ± 22.1)	...	...
2.....	3 43 09.28 ± 0.11	31 15 13.1 ± 1.3	2326.8 ± 73.3	(2255.1 ± 68.7)	...	...
9.....	3 44 00.78 ± 0.14	31 38 15.3 ± 2.7	471.7 ± 19.2	(471.8 ± 15.9)	...	...
10.....	3 44 10.03 ± 0.14	32 29 22.8 ± 2.5	426.0 ± 18.8	(426.1 ± 14.3)	...	...
12.....	3 44 16.96 ± 0.22	31 53 35.5 ± 4.1	387.4 ± 35.0	(348.6 ± 13.7)	...	...
8.....	3 44 32.56 ± 0.13	32 12 39.9 ± 2.2	753.5 ± 27.2	(632.6 ± 20.3)	...	...

Note.—Units of right ascension are hours, minutes, and seconds, and units of declination are degrees, arcminutes, and arcseconds.

[a] Position angle north of east.

and show no discernible enhancement at the location of the ring.

3.3. *The IRAS Ring*

In Figure 4, we show maps of $\tau_{\rm dust}$ and $T_{\rm dust}$ for the area of the *IRAS* ring. As can be seen, there is a depression in the opacity of dust toward and to the northwest of HD 278942. The observed *IRAS* ring shows up as an increase in dust optical depth. The temperature map shows that the ring is at a temperature minimum of $\approx$24 K and the dust toward the immediate area surrounding the star is at higher temperatures.

The *IRAS* Point Source Catalog (PSC) shows a weak source at the center of the extended structure coinciding with the star. We have rederived the photometry toward the central, compact source, based on the FRESCO data, by "on-chip" photometry. Because the shape and size of the compact source vary rather dramatically from 12 to 100 μm, we used only a single aperture in IRAF-APPHOT with a radius of 2.25 and an annulus between 3.75 and 5′ for the background subtraction. We chose this aperture as it matches the beam size of the 100 μm channel. In Table 3, we list our derived fluxes for the compact source as well as those from the PSC. We note that although the derived *IRAS* fluxes depend on the size of the aperture, the colors are close to constant for apertures at least as large as $r =$ 5.75. The uncertainties quoted in Table 3 for the four *IRAS* bands have been increased over the formal errors in the

TABLE 2

1420 MHz Sources

Source	R.A. (J2000)	Decl. (J2000)	Integrated Flux (mJy)	Peak Flux (mJy)	Size (arcsec)	P.A.[a] (deg)
3.....	3 37 37.14 ± 0.10	32 08 01.6 ± 1.1	82.7 ± 2.7	77.8 ± 2.4	0.5 × 0.2	174
2.....	3 37 49.78 ± 0.10	31 15 13.1 ± 1.0	124.7 ± 4.0	124.7 ± 3.8	...	...
6.....	3 37 50.76 ± 0.10	32 02 08.9 ± 1.1	45.6 ± 1.6	45.6 ± 1.4	...	...
7.....	3 38 04.71 ± 0.10	31 36 29.5 ± 1.1	35.7 ± 1.2	35.7 ± 1.1	...	...
9.....	3 38 33.88 ± 0.10	32 22 25.4 ± 1.1	33.9 ± 1.2	33.9 ± 1.1	...	...
5.....	3 39 58.94 ± 0.10	32 21 04.9 ± 1.1	49.6 ± 1.6	49.7 ± 1.5	...	...
10	3 40 06.48 ± 0.10	31 28 24.0 ± 1.1	31.5 ± 1.1	31.5 ± 1.0	...	...
1.....	3 40 08.44	32 09 00.5	1429.2 centroid	...	...	...
1A.....	3 40 08.47 ± 0.13	32 08 59.3 ± 2.6	1416.8 ± 92.2	1217.1 ± 76.7	0.9 × 0.0	22
1B.....	3 40 07.05 ± 1.14	32 09 46.1 ± 57.9	30.3 ± 97.7	29.8 ± 95.9	...	...
4.....	3 41 31.30 ± 0.10	32 24 57.7 ± 1.1	67.4 ± 2.2	66.7 ± 2.1	...	...
8.....	3 41 41.07	31 23 07.8	57.2 centroid	...	...	...
8A.....	3 41 40.38 ± 0.39	31 23 00.8 ± 5.5	40.7 ± 6.2	32.1 ± 4.3	0.7 × 0.5	57
8B.....	3 41 43.14 ± 0.50	31 23 17.5 ± 19.3	12.7 ± 6.1	11.8 ± 5.2	...	...
8C.....	3 41 40.29 ± 1.37	31 23 52.4 ± 11.9	4.2 ± 3.6	4.2 ± 3.6	...	...
11	3 42 03.46 ± 0.10	31 27 03.9 ± 1.2	34.4 ± 1.4	32.3 ± 1.1	...	...
12	3 43 23.17 ± 0.10	31 36 40.4 ± 1.1	30.3 ± 1.0	30.3 ± 1.0	...	...

Note.—Units of right ascension are hours, minutes, and seconds, and units of declination are degrees, arcminutes, and arcseconds.

[a] Position angle north of east.

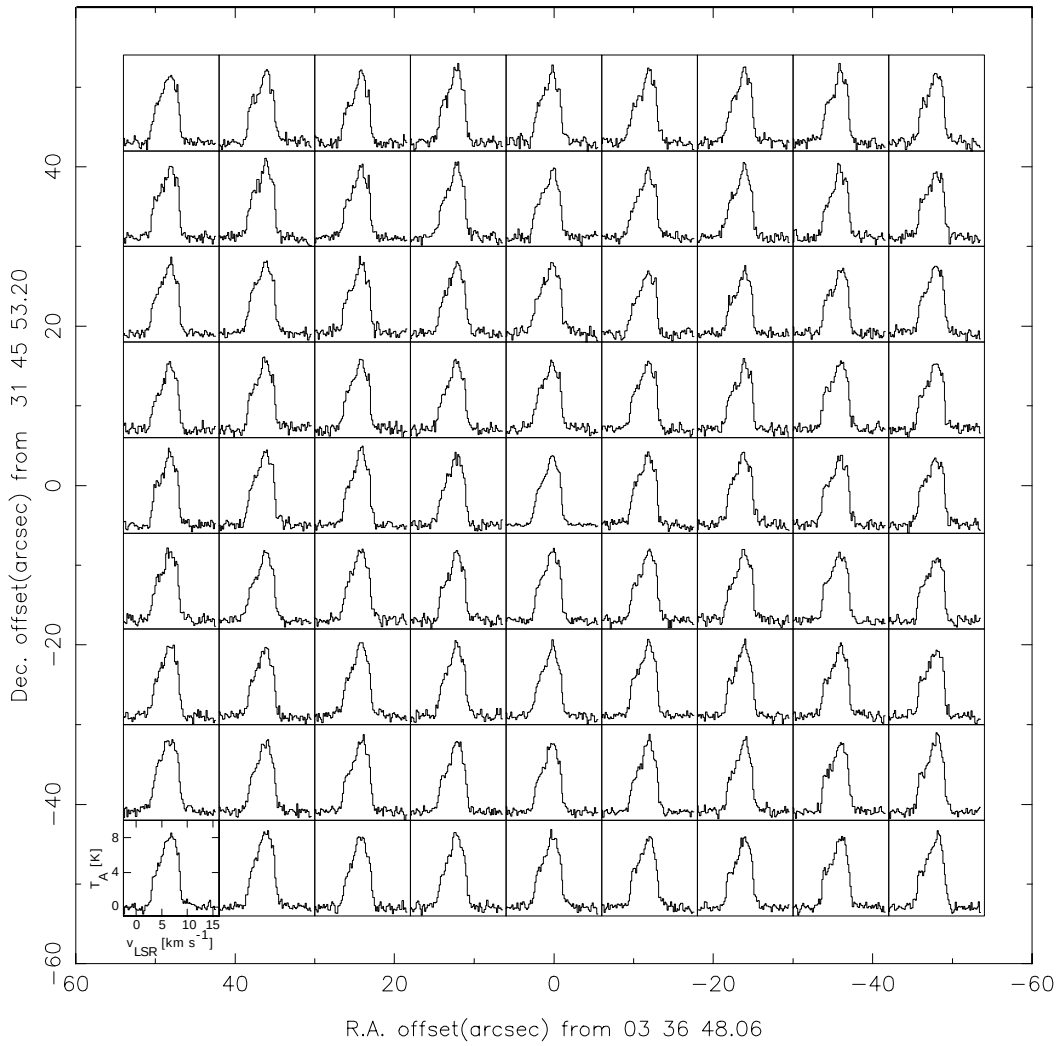

FIG. 3*a*

FIG. 3.—Grids of (*a*) ^{12}CO $J = 2$–1 and (*b*) ^{13}CO $J = 1$–0 spectra in the area of HD 278942 show no obvious contribution from circumstellar material

photometry. To account for the high and varying background, we multiplied the formal (Poisson) errors by the ratio of the average, background-subtracted pixel value inside the aperture and the average pixel value in the sky annulus. In Figure 5, we show a blackbody fit to the data points. As can be seen, the data can be well described by a Planck function of $T = 65 \pm 2$ K.

3.4. *Diffuse Visible Light Image and Star Counts*

In Figure 6, we show an 1°.5 × 1°.5 image extracted from the POSS-II data using the Digital Sky Survey (DSS) archive at STScI.[10] Contours for the dust opacity have been overlaid to show the relative location of the features. The optical figure consists of a mosaic of nine subfields from the DSS, a few of which were scaled by up to 15% to avoid high-contrast steps between the subfields. The strong brightness enhancement in the eastern end of the image is caused by the open cluster and reflection nebula IC 348. As can be seen, an irregular region of diffuse emission exists around and to the northwest of HD 278942 (upon which the image is centered) together with several patches of higher opacity material. Comparing this with the *IRAS* data, we see that the diffuse emission coincides with the area of lower dust opacity. Several of the features in the diffuse image can be correlated with the star counts of Cernicharo & Bachiller

TABLE 3

DERIVED FIR FLUXES FOR THE COMPACT SOURCE

λ (μm)	*IRAS* PSC (mJy)	FRESCO/JCMT (mJy)
12	0.46 ± 0.03	1.08 ± 3.2
25	1.68 ± 0.20	13.02 ± 2.1
60	<9.56	26.9 ± 1.5
100.....	<19.25	15.8 ± 2.9
850.....	...	<0.73

[10] The Digitized Sky Surveys were produced at the Space Telescope Science Institute under US Government grant NAG W-2166. The images of these surveys are based on photographic data obtained using the Oschin Schmidt Telescope on Palomar Mountain and the UK Schmidt Telescope. The plates were processed into the present compressed digital form with the permission of these institutions. The Second Palomar Observatory Sky Survey (POSS-II) was made by the California Institute of Technology with funds from the National Science Foundation, the National Geographic Society, the Sloan Foundation, the Samuel Oschin Foundation, and the Eastman Kodak Corporation.

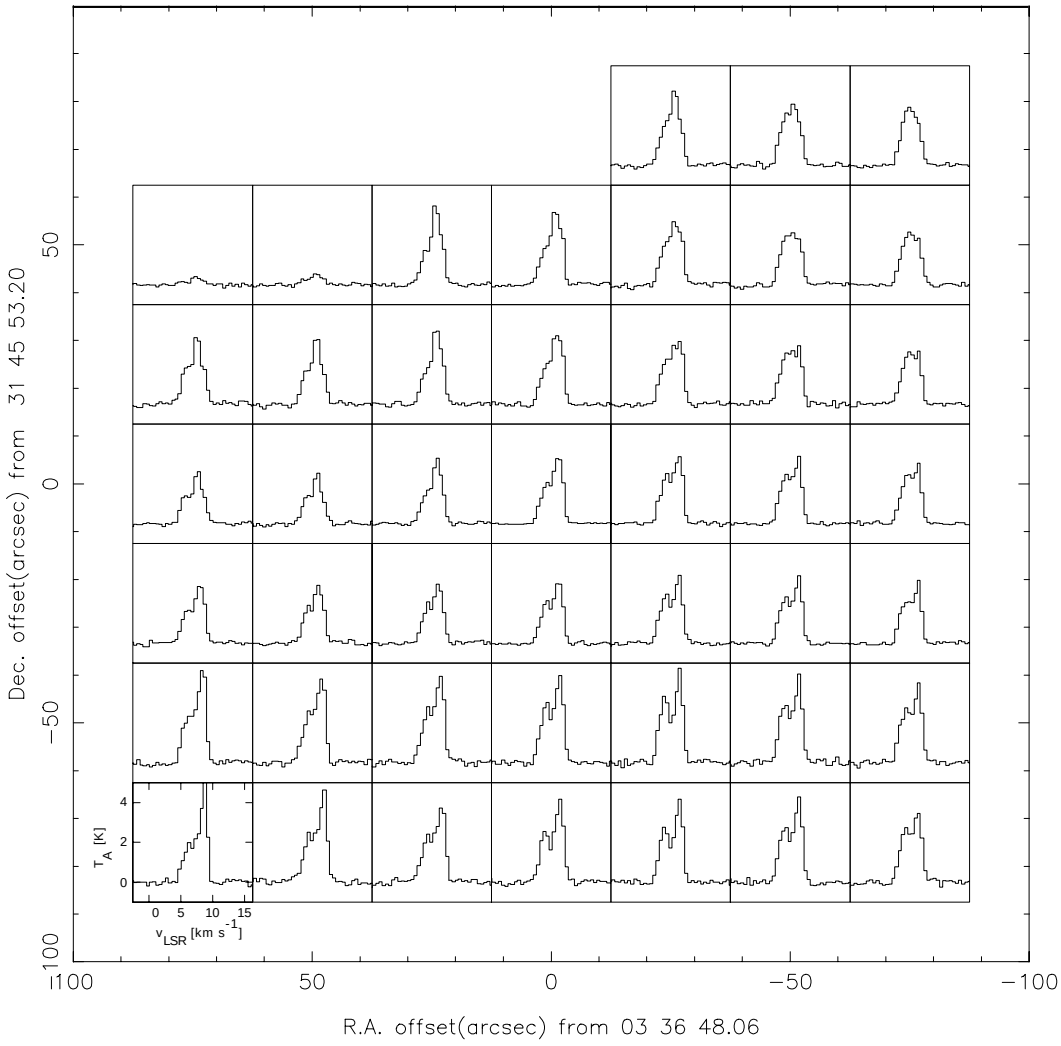

FIG. 3*b*

(1984). Most prominently, the dark lane running diagonally from directly north of HD 278942 and to the southeast, and then due eastward, shows up as a region of enhanced visual extinction in the star-count data. However, neither the location of the star nor the *IRAS* ring show any increase in extinction in the star-count data. A decrease is seen in the region of low 100 μm opacity. The star counts in the immediate vicinity of HD 278942 yield a visual extinction of only about 2.5 mag.

3.5. *The Star HD 278942*

We have performed spectroscopy, photometry, and polarimetry of the star HD 278942. Our results are summarized in Table 4.

3.5.1. *Visual Spectroscopy*

The visual wavelength spectroscopic data allow a spectral classification to be made as well as several interstellar species to be measured (Fig. 7). In Table 5, we have listed the equivalent widths of some of the lines most sensitive to variations in spectral class of late O stars and early B stars. As can be seen, a spectral class between O9 and B0 is most consistent with the measurements. The nondetection of He II would indicate that B0 is the more appropriate classification.

Based on the equivalent width of the Hγ line (Millward & Walker 1985), $W_{H\gamma} = 2.5 \pm 0.1$, we find an absolute magnitude of $M_V = -4.9 \pm 0.1$. This is somewhat bright for a main-sequence B0 star, which more typically has an $M_V \approx -4.0$ (Schmidt-Kaler 1982). However, preliminary analysis using line synthesis techniques (A. W. Fullerton, 1999, private communication) shows significant discrepancies between the observed Hα and Hβ lines and models of B giant atmospheres, indicating a higher surface gravity than for giants. Hence, we assign a preliminary spectral class of

TABLE 4

DERIVED STELLAR PARAMETERS FOR HD 278942

Parameter	Value
Spectral Class	O9.5–B0 V
m_V	8.83 ± 0.01 mag[a]
$B-V$	1.44 ± 0.01 mag
M_V	−4.9 ± 0.1 mag
E_{B-V}	1.75 mag ($A_V = 5.5 - 7.6$ mag for $R = 3.1$–4.3)
v_{LSR}	28 ± 1 km s^{-1}
$v \sin i$	125 ± 20 km s^{-1}

[a] Černis 1993 reports $m_V = 9.10 \pm 0.01$ and $(B-V) = 1.34$ based on Vilnius photometry.

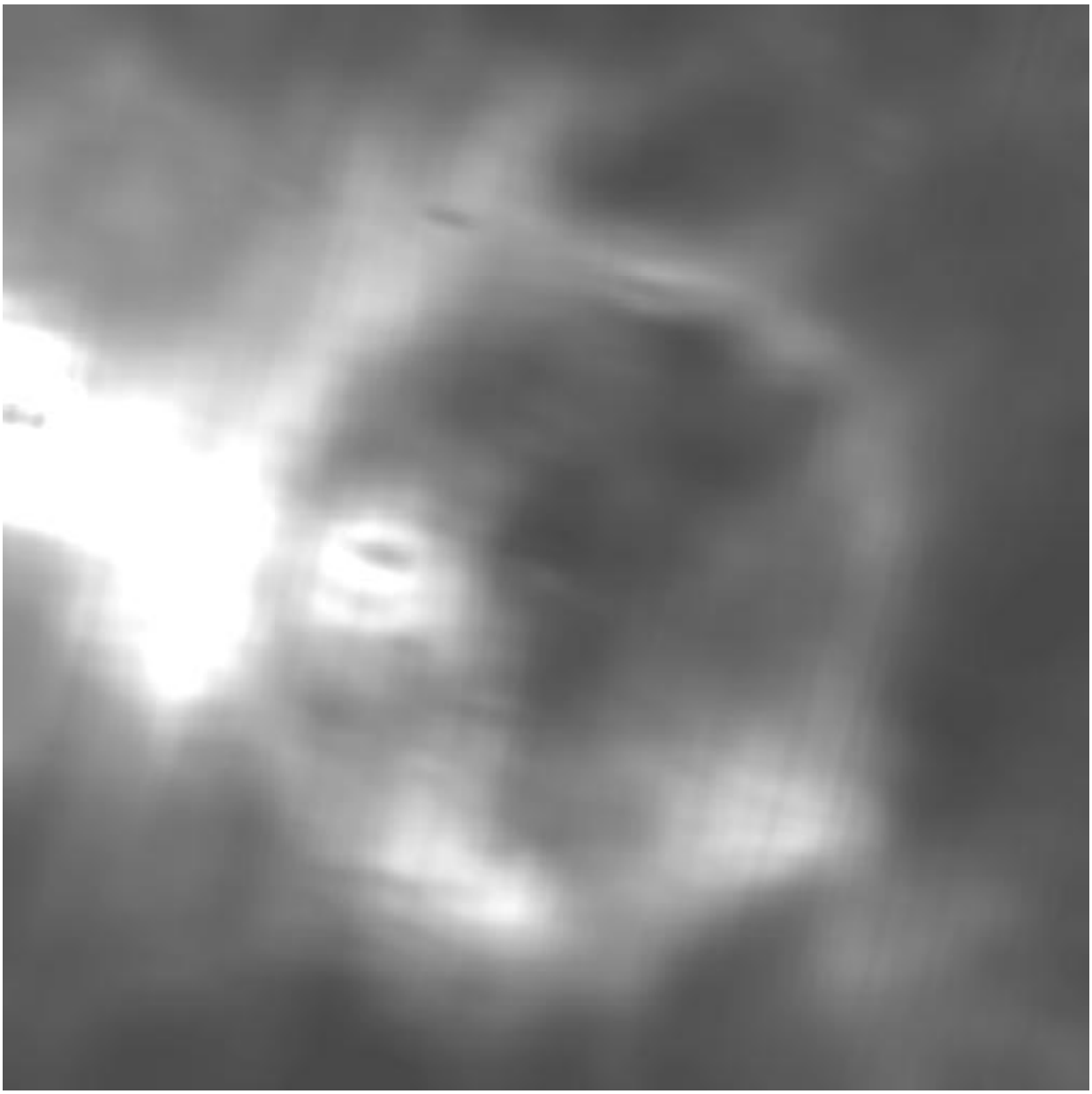

FIG. 4*a*

FIG. 4.—Opacity and temperature of the *IRAS* ring region were derived using the algorithms of Kuiper et al. 1987. Each panel is a 2° field centered on HD 278942. (*a*) shows the dust opacity while (*b*) shows dust temperature. In both cases, brighter gray scale corresponds to larger values. For most of the pixels, the dust opacity varies between 0 and 0.2. The temperature varies between 21 and 31 K.

O9.5–B0 V while noting the above inconsistencies. We defer detailed modeling of the stellar spectrum to a later paper.

If we use the derived luminosity and surface gravity to indicate the earlier spectral class of O9.5 V, we may use the stellar evolution tracks from Schaller et al. (1992) to derive a stellar age. Assuming a solar metallicity, we find an age of about 8 Myr. This estimate is similar to the estimated age of the Per OB2 association (Giménez & Clausen 1994), while somewhat older than the estimated age of the nearby open cluster IC 348 (Herbig 1998).

Based on the Si III triplet at $\lambda\lambda$4552.6, 4567.8, and 4574.8, we find a LSR velocity for the star of $v_{\rm LSR} = 28 \pm 1$ km s^{-1}, which may be compared with the interstellar absorption velocities of $v_{\rm LSR} = 8$ km s^{-1} for CH (λ4300) and C_2 (Q(2); λ8761) and $v_{\rm LSR} = 6$ km s^{-1} for Ca II and Na I. The millimeter-wave CO emission in the direction of the star is centered at about 7 km s^{-1}. Finally, using the FWHM of He I lines at 4026 and 4388 Å (the line at 4471 Å was excluded because of severe blending) and their relation to rotational velocity (Gray 1992, p. 378), we find $v \sin i = 125 \pm 20$ km s^{-1}.

3.5.2. *Photometry*

From the photometric measurements, we find a V magnitude of 8.83 $\pm$ 0.01 and a B magnitude of 10.27 $\pm$ 0.01. For comparison, Černis (1993) found $V = 9.10 \pm 0.012$. If we use the relation between colors in the Vilnius system and $(B-V)$ (Straižys 1992),

$$B-V = -0.33 + 0.50[(X-V) + (Y-V)] , \qquad (1)$$

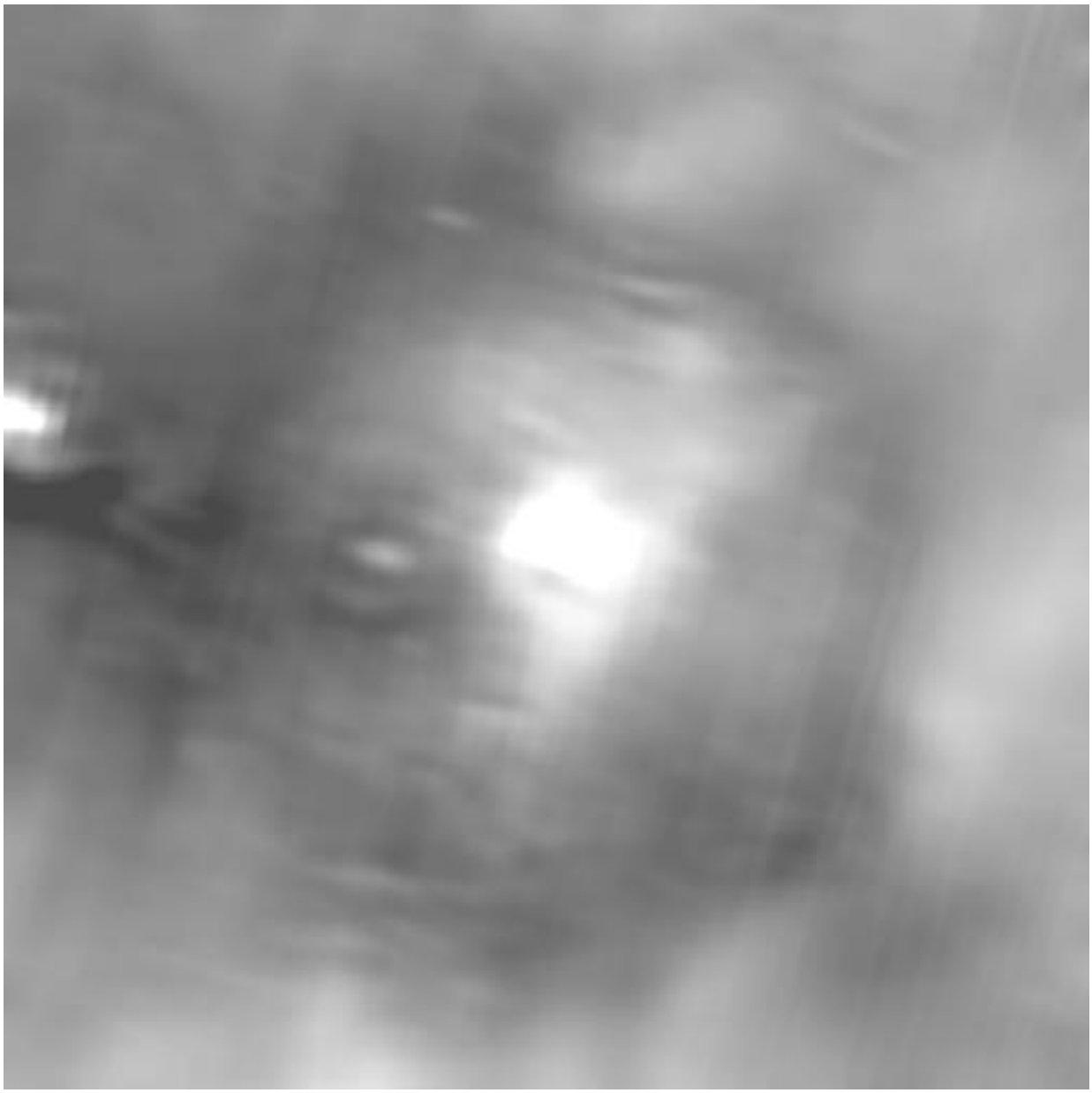

FIG. 4*b*

TABLE 5

EQUIVALENT WIDTHS FOR HD 278942 AND STANDARDS[a]

Line	HD 278942	O8	O9	B0	B2
Hα	2.3 ± 0.2	...	...	3.8	6.0
Hβ	2.5 ± 0.2	...	...	3.8	6.0
Hγ	2.4 ± 0.3	2.2	2.6	3.5	5.1
He I (λ4471)	0.7 ± 0.1	0.9	1.0	1.0	1.3
He I (λ4026)	0.9 ± 0.1	0.7	0.9	1.0	1.3
He I (λ4388)	0.6 ± 0.1	0.4	0.45	0.8	...
He II (λ4541)	<0.08	0.6	0.4	...	...
Mg II (λ4481).....	0.07 ± 0.005	...	...	0.1	0.2
C II (λ4267).....	0.08 ± 0.01	...	...	0.05	0.2
Si IV (λ4089).....	0.06 ± 0.01	0.3	0.35	0.2	0

[a] From Peterson & Scholz 1971; Conti 1973; Didelon 1982; and Jaschek & Jaschek 1987, p. 137.

we find that Černis's results correspond to $B = 10.44$. K. Černis (1997, private communication) reports having detected no variability for the star in his set of four separate measurements between 1985 and 1991. We note that our application of equation (1) is in a range outside of the stated validity range of $B-V < 0.8$. The derived spectral class yields an intrinsic color of $(B-V)_0 = -0.30 \pm 0.01$ (Straižys 1992) and, hence, a color excess of $E_{B-V} = 1.75$.

3.6. *Interstellar Polarization and Absorption toward HD 278942*

Several interstellar atomic and molecular lines were detected in the spectrum of HD 278942, including those of Na I, Ca II, CH, and CH^+. Here we will concentrate solely on the measurements of the C_2 Phillips band at 8757–8782 Å since these lines allow us to derive an estimate of the

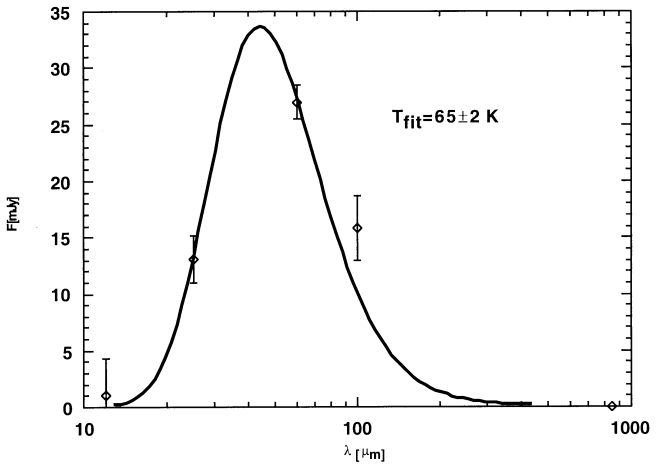

FIG. 5.—Results of the "on-chip" aperture photometry of source at the location of HD 278942, using the *IRAS* FRESCO data together with 850 μm SCUBA photometry, fitted to a blackbody function. Best fit yields a temperature of 65 ± 2 K.

kinetic temperature of the intervening gas. In Figure 8, we show the C_2 spectrum against the background of the Paschen-ι line of the star. In Table 6, we list the measurements and derived values for the C_2 observations, assuming a nominal b value of 1.0 km s^{-1}. In those cases where two C_2 lines are blended, e.g., $R(4)$ and $R(8)$, we performed constrained fits of the spectrum, imposing the measured wavelength separation of the lines and a common line width.

TABLE 6

C_2 ANALYSIS

Line	λ[a] (Å)	f[b]	W (mÅ)	N[c] (10^{13}cm^{-2})
$R(0)$	8757.686	1.0×10^{-3}	13.3 ± 0.3	2.2 ± 0.5
$N(0)$	...	...	...	2.2 ± 0.5[d]
$R(2)$	8753.949	4.0×10^{-4}	15.0 ± 0.3	6.2 ± 0.2
$Q(2)$	8761.194	5.0×10^{-4}	17.0 ± 0.4	5.7 ± 0.2
$P(2)$	8766.031	1.0×10^{-4}	3.9 ± 0.3	5.9 ± 0.5
$N(2)$	...	...	...	5.9 ± 0.2[d]
$R(4)$	8751.685	3.33×10^{-4}	7.9 ± 0.3	3.7 ± 0.2
$Q(4)$	8763.751	5.0×10^{-4}	13.8 ± 0.5	4.5 ± 0.2
$P(4)$	8773.430	1.67×10^{-4}	3.3 ± 0.3	3.0 ± 0.3
$N(4)$	...	...	...	3.9 ± 0.6[d]
$R(6)$	8750.848	3.08×10^{-4}	3.9 ± 0.2	1.9 ± 0.1
$Q(6)$	8767.759	5.0×10^{-4}	7.9 ± 0.4	2.5 ± 0.1
$P(6)$	8782.308	1.92×10^{-4}	3.4 ± 0.2	2.7 ± 0.2
$N(6)$	...	...	...	2.3 ± 0.3[d]
$R(8)$	8751.486	2.94×10^{-4}	1.7 ± 0.3	0.9 ± 0.2
$Q(8)$	8773.221	4.99×10^{-4}	5.6 ± 0.5	1.7 ± 0.2
$N(8)$	...	...	...	1.3 ± 0.4[d]
$R(10)$	8753.578	2.86×10^{-4}	2.5 ± 0.3	1.3 ± 0.2
$Q(10)$	8780.141	4.99×10^{-4}	2.3 ± 0.3	0.7 ± 0.1
$N(10)$	...	...	...	0.8 ± 0.3[d]
$Q(12)$	8788.559	4.98×10^{-4}	1.4 ± 0.4	0.4 ± 0.1
$N(12)$	...	...	...	0.4 ± 0.1[d]
$Q(14)$	8788.559	4.98×10^{-4}	0.9 ± 0.5	0.3 ± 0.2
$N(14)$	...	...	...	0.3 ± 0.2[d]
$Q(16)$	8788.559	4.97×10^{-4}	1.5 ± 0.3	0.4 ± 0.1
$N(16)$	...	...	...	0.4 ± 0.1[d]

[a] From van Dishoeck & de Zeeuw 1984.
[b] From Federman et al. 1994.
[c] Assuming $b = 1.0$ km s^{-1}.
[d] Best estimate of the column densities in each J level, derived by averaging the measurements of the lines originating in each level.

The excitation in the electronic ground state of C_2 is influenced by the strength of the infrared radiation field through the fluorescence between the $X\ ^1\Sigma_g^+$ and the $A\ ^1\Pi_u$ states (van Dishoeck & Black 1982). Therefore, the detailed interpretation of the level populations of the rotational ladder is somewhat model dependent through the factor $n\sigma/I_{IR}$, where n is the density of collision partners, σ is the collision cross section and I_{IR} is a dimensionless scaling for the local infrared radiation field relative to the average interstellar field (see van Dishoeck & Black 1982 for details). However, we can form two estimates of the kinetic temperature in the gas. The simplest consists of the direct excitation temperature between the $J = 2$ and $J = 0$ levels, for which we derive an excitation temperature of 26 ± 5 K. A more complete analysis (cf. Federman et al. 1994) yields a best fit for all the measured level populations of $T = 20 \pm 10$ K and $n\sigma/I_{IR} = (7 \pm 2) \times 10^{-14}$ cm^{-1}. For a cross section of 2×10^{-16} cm^2 (van Dishoeck & Black 1982), this corresponds to $n/I_{IR} = 350$ cm^{-3}. Given that the infrared radiation field of the region is likely to be higher than normal, $n = 350$ cm^{-3} must be viewed as a lower limit to the actual space density of the C_2 bearing gas.

3.6.1. *Polarimetry*

The polarization measurements show a polarization curve that increases monotonically from the B to I bands (Fig. 9), while flattening off toward the infrared. The angle of polarization stays constant to within the measurement uncertainties. The R-band polarization of 5.9 ± 0.03%, at an angle of 154°.0 ± 0°.2 (east of north) is consistent, both in magnitude and in direction, with the most highly polarized sources in the Perseus complex, as measured by Goodman et al. (1990), as well as the (red) polarization of BD +31°643 (Andersson & Wannier 1997).

The maximum of the polarization curve has been shown to be related to R, the ratio of total-to-selective extinction (Whittet & van Breda 1987). We therefore used the Serkowski relation (e.g., Whittet 1992, p. 93) to find the wavelength of maximum polarization. The formally best solution yields $\lambda_{max} = 0.76 \pm 0.01$ μm. The uncertainty in this value is only from the formal fitting uncertainty. The true values of both λ_{max} and $\sigma_{\lambda_{max}}$ are likely to be larger since we do not have any near-infrared data and the observed polarization curve does not conform well to a standard Serkowski shape. Using the relationship between λ_{max} and R from Whittet & van Breda (1987), we find $R = 4.3 \pm 0.2$.

4. DISCUSSION

4.1. *The Physical Nature of the IRAS Ring and Its Surroundings*

4.1.1. *The IRAS Ring and Its Origin*

We used the maps of the four *IRAS* bands to compare the location of the diffuse far-infrared (FIR) emission and that of HD 278942. From *IRAS* ratio maps, we extracted one-dimensional cuts in the four canonical directions. In each case, the center of the *IRAS* ring fell within 5′ of the map center (location of HD 278942). Hence the geometry of the *IRAS* ring and the location of the star HD 278942 strongly indicate that the latter is responsible for the former. That the ring observationally is caused by an opacity enhancement and is filled by warm dust indicates that it is the result of an expanding stellar wind. The identification of HD 278942 as an O9.5–B0 V star at the ring's geometric center supports this conclusion in that stars of this type are known

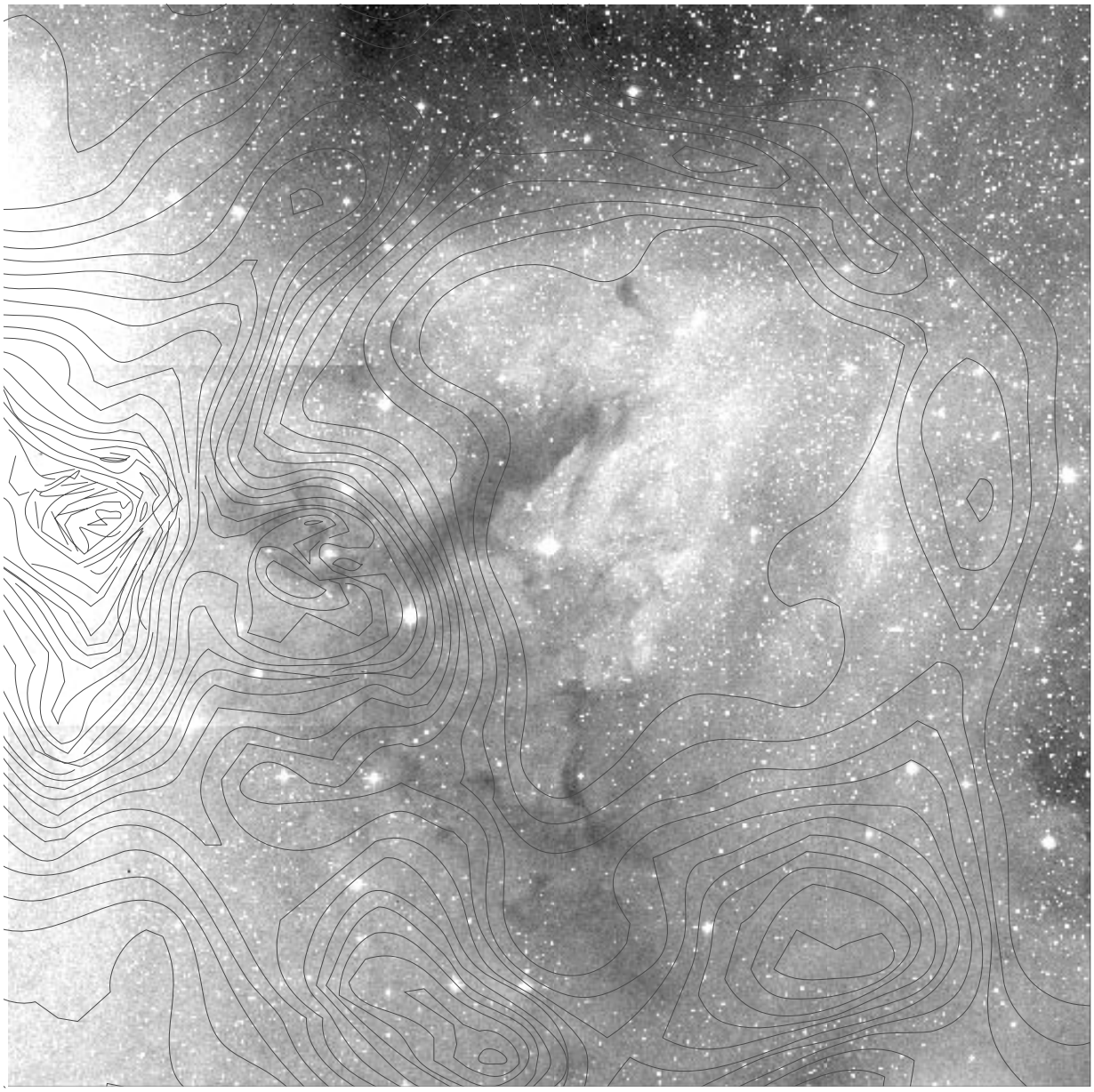

FIG. 6.—A 1°.5 × 1°.5 excerpt from the POSS-II, extracted from the DSS archive at STScI, is shown together with contours for the dust opacity. The image is centered on HD 278942. Note the presence of several patches of high opacity to the east of the star.

to have fast stellar winds with mass-loss rates of the order of $10^{-7}\ M_{\odot}\ \mathrm{yr}^{-1}$ (Lamers & Leitherer 1993 and references therein).

4.1.2. *The Diffuse Emission and Its Excitation*

The flat spectrum of the diffuse radio source suggests that the emission is caused by optically thin thermal radiation. As can be seen from Figure 6, the diffuse Hα emission closely coincides with the low dust-opacity region in the western part of the *IRAS* maps, and lower surface intensity emission can be seen to the northwest of the brightest part. A comparison with published large-scale CO maps of the region (e.g., Cernicharo & Bachiller 1986) shows that the star is located close to the ^{13}CO edge of the cloud at a place where the local CO gradient is oriented in a roughly east-to-southeast direction. Another interesting comparison can be made with the maps of H I (21 cm) emission from Wannier et al. (2000). Figure 10 shows a single-channel map of H I (21 cm) emission at $v_{\mathrm{LSR}} = 10\ \mathrm{km\ s}^{-1}$, in which we have also marked the approximate location of HD 278942. This velocity corresponds to the center velocity of the molecular gas in the B5 region (at the easternmost extent of the Perseus complex), while it is somewhat redder than the CO velocity at the location of B1 (Ungerechts & Thaddeus 1987; Wannier et al. 2000). Immediately to the northwest of the *IRAS* ring, a pincerlike feature can be seen in the atomic hydrogen emission. These H I observations suggest that the H II region around HD 278942 has broken through the cloud to the northwest and is venting its ionized gas into the low-density surroundings. The dark patches seen in the optical image, as well as the star-count data, suggest that the center of the blister is located somewhat behind the

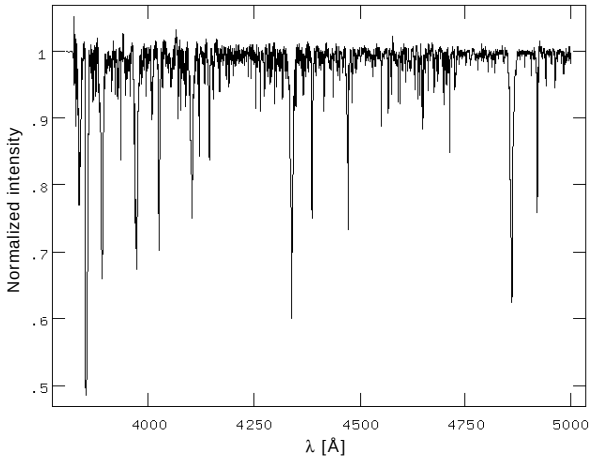

FIG. 7.—We observed HD 278942 with the coudé spectrograph at the 2.8 m telescope at the McDonald Observatory. This echelle spectrum of HD 278942 yields a O9.5–B0 V spectral classification. We have used line ratios of a number of tracers to derive the spectral class and some fundamental stellar parameters, such as radial velocity and stellar rotation (see Table 4).

midplane of the cloud, a view supported by the kinematics of large-scale H I observations of the region (Wannier et al. 2000).

The diffuse radio continuum emission is clearly strongest in the eastern part of the *IRAS* ring. Given the combined data sets, we feel that the most natural interpretation of the measured radio fluxes is that we have somewhat more missing flux in our higher frequency 1420 MHz data than in our 408 MHz data and that the spectral index is indicative of an optically thin H II region. The distribution of the diffuse radio emission can then be understood as the continued interaction of the stellar UV radiation with the remaining parent cloud. However, our data are also consistent with a spectral energy distribution rising at longer wavelengths, indicating a possible nonthermal component (cf. Pauls 1999). We will not explore this second possibility in detail here but note in passing that in a strong stellar wind some nonthermal emission is possible owing to an interaction of the wind with the remaining molecular cloud or from shocks within the wind (White 1985; Bieging, Abbott, & Churchwell 1989). Whether such a mechanism would be able to produce the observed radiation is unclear and will require a more complete analysis of all the available radio data.

4.2. *The Star and Its Immediate Surroundings*

The high color excess of the star indicates heavy obscuration. Using the derived R value of 4.3, a visual extinction of $A_V = 7.4$ mag is found. Since Perseus is the only major source of extinction in the direction (Černis 1993), and recognizing the nonstandard shape of the polarization curve from which R was derived, we may turn the argument around and ask what value of R is found from the measured colors and assume the star to be at the distance of the Perseus complex (260 pc; Černis 1993). We note that the *Hipparcos* datum for the star, 207 ± 52 pc (ESA 1997), is consistent with the photometric distance. With this distance estimate and $M_V = -4.9$ mag, we find $R = 3.8$ ($A_V = 6.7$). Considering the uncertainty in the fit for λ_{max}, this is quite good agreement. We may therefore safely conclude that HD 278942 is indeed located within the Perseus molecular cloud.

The large-scale extinction, as measured by star counts, shows a significantly lower value toward the star. Even though star counts can severely underestimate the average extinction in a patchy region, the existence of a strong compact source in the shorter *IRAS* bands at the location of the star would seem to indicate a circumstellar term in the visual extinction besides the diffuse contributions.

4.2.1. *A Possible Circumstellar Disk*

A high degree of linear polarization suggests a nonisotropic geometry for the source (e.g., Bastien & Ménard 1990). The recent detection of a dust disk around the B5 V star BD +31°643 in IC 348 makes the polarization measurements of HD 278942, taken together with the *IRAS* and millimeter-wave data, all the more intriguing as an indicator of a possible circumstellar disk. In the case of BD +31°643, aperture polarimetry shows a polarization that is parallel to the major axis of the projected disk and is perpendicular on the sky to the projected direction of the local magnetic field (Andersson & Wannier 1997). The magnetic

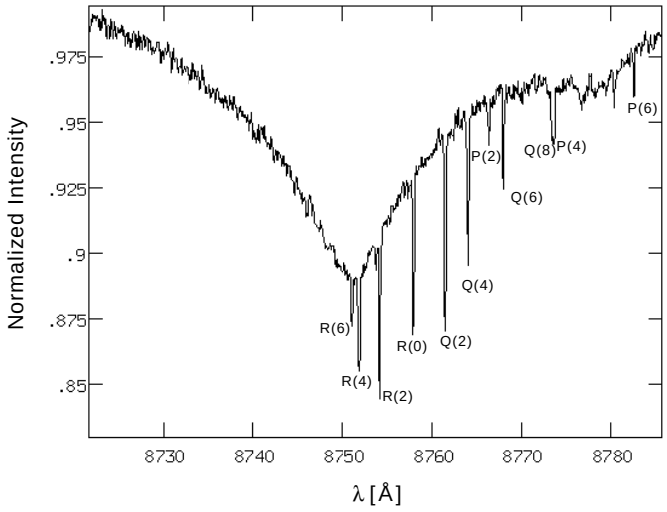

FIG. 8*a*

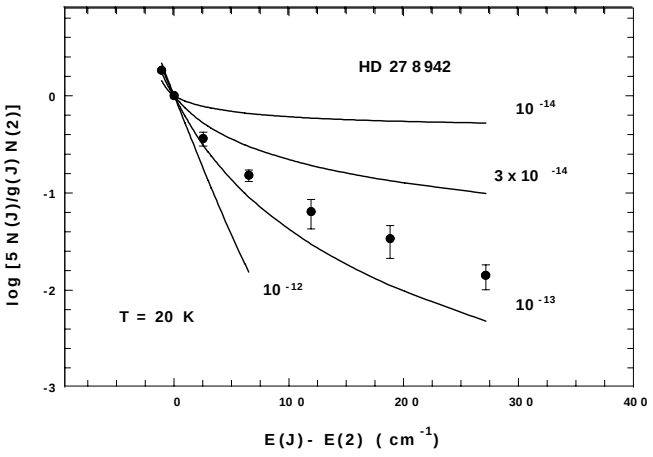

FIG. 8*b*

FIG. 8.—(*a*) Against the backdrop of the Paschen-ι line of the star, the interstellar lines from the Phillips band of C_2 can be detected up to $Q(16)$. (*b*) After normalizing out the stellar line, the C_2 lines were analyzed to yield a gas temperature of 20 ± 10 K and a space density of $n_H \geq 350$ cm^{-3}.

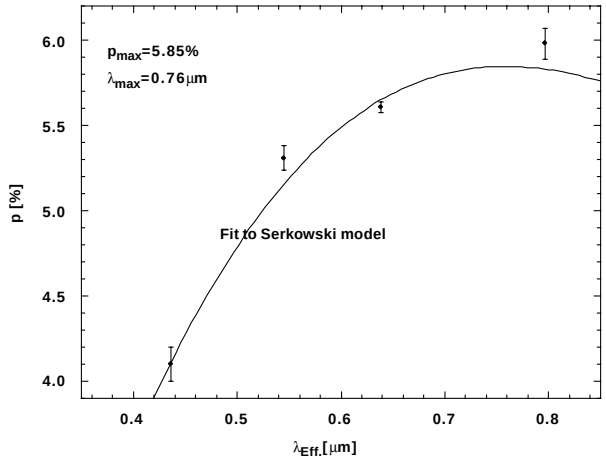

FIG. 9.—Multiband polarimetry of HD 278942 reveals a nonstandard polarization curve, monotonically rising toward the red. The direction of polarization is found to be constant for all four bands at $\theta = 154°$.

field in the vicinity of HD 278942 seems, based on polarization measurements in the cloud halo (Wannier & Andersson 1996), to be similarly directed along the long axis of the cloud complex. As for BD +31°643, the polarization of HD 278942 is perpendicular to this field direction. That our *IRAS* photometry yields quite a good fit to a 65 K blackbody indicates the presence of heated dust around the star. That no circumstellar CO emission is detected, as well as the significantly lower excitation temperature of C_2, compared with the dust, in turn indicates the possibility of a circumstellar dust disk rather than a gaseous circumstellar envelope. The recent discovery of a circumstellar disk around the embedded O9 star G339.88−1.26 by Stecklum et al. (1998)[11] lends added credence to this hypothesis. Hence, we suggest that the high-mass, main-sequence star HD 278942 may have a circumstellar disk.

5. CONCLUSION

We have shown that the star HD 278942 is a heavily obscured O9.5–B0 V star located at the geometric center of the *IRAS* ring G159.6−18.5. Based on spectroscopy, photometry, and polarimetry, we argue that this superposition is not accidental but that the star is embedded in the Perseus molecular cloud and is indeed responsible for the *IRAS* feature. A faint, flat spectrum extended radio source is found at the location of the *IRAS* ring as well as diffuse Hα emission at and to the northwest of the star. The extent of the latter coincides with a depression in the 100 μm opacity, and we interpret this as the result of a ruptured H II blister, i.e., an H II region expanding past the boundary of the enclosing cloud. An intriguing possibility, suggested by the direction of the polarization vectors and the *IRAS* point-source measurements, is that HD 278942 has a circumstellar disk similar to that recently detected around BD

[11] ESO press release available at http://www.eso.org/outreach/press-rel/pr-1998/pr-08-98.html.

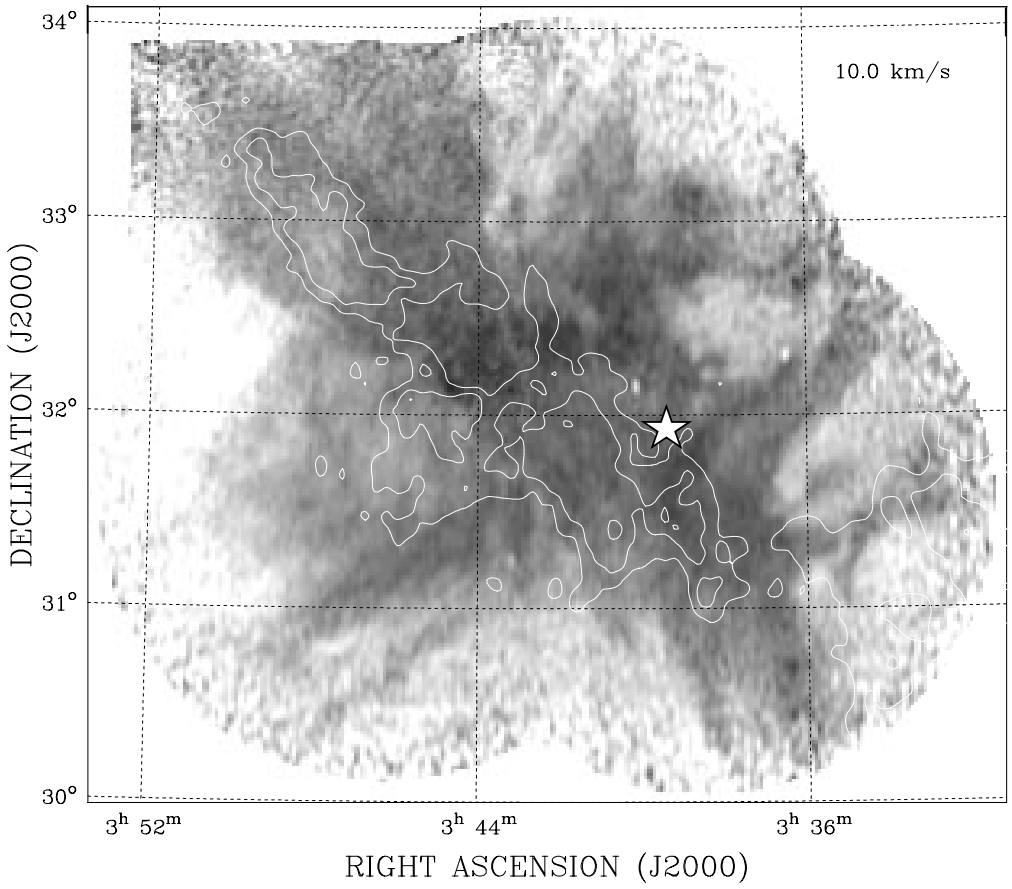

FIG. 10.—Single-channel map of atomic hydrogen emission (gray scale) and CO $J = 1–0$ (white contours) from Wannier et al. 2000 at $v_{LSR} = 10$ km s^{-1} shows some of the interaction of HD 278942 and its host cloud. Note, in particular, the pincerlike feature to the northwest of the star (see text).

+31°643 (Kalas & Jewitt 1997; Andersson & Wannier 1997).

It is a pleasure to acknowledge the staffs at each of the observatories used for this study for their skilled and generous support. We gratefully acknowledge A. W. Fullerton and S. R. Federman for helpful discussions and the use of their analysis routines. The referee, T. Pauls, provided several comments and suggestions that helped to improve the paper. This work was, in part, carried out at the Jet Propulsion Laboratory, California Institute of Technology, under contract with the National Aeronautics and Space Administration.

REFERENCES

Andersson, B.-G., & Wannier, P. G. 1996, ApJ, 443, L49
———. 1997, ApJ, 491, L103
Aspin, C., Sandell, G., & Russell, A. P. G. 1994, A&AS, 106, 165
Bastien, P., & Ménard, F. 1990, ApJ, 364, 232
Bieging, J. H., Abbott, D. C., & Churchwell, E. B. 1989, ApJ, 340, 518
Breger, M. 1979, ApJ, 233, 97
Cernicharo, J., & Bachiller, R. 1984, A&AS, 58, 327
———. 1986, A&A, 166, 283
Cernicharo, J., Bachiller, R., & Duvert, G. 1985, A&A, 149, 273
Černis, K. 1993, Baltic Astron., 2, 214
Conti, P. S. 1973, ApJ, 179, 161
de Zeeuw, P. T., Hoogerwerf, R., Bruijne, J. H. J., Brown, A. G. A., & Blaauw, A. 1999, AJ, 117, 354
Didelon, P. 1982, A&AS, 50, 199
ESA. 1997, The *Hipparcos* and Tycho Catalogs (ESA SP-1200) (Noordwijk: ESA)
Federman, S. R., Strom, C. J., Lambert, D. L., Cardelli, J. A., Smith, V. V., & Joseph, C. L. 1994, ApJ, 424, 772
Fiedler, R., Pauls, T., Johnston, K. J., & Dennison, B. 1994, ApJ, 340, 595
Fomalont, E. B. 1989, in ASP Conf. Ser. 5, Synthesis Imaging in Radio Astronomy, ed. R. A. Perley, F. R. Schwab, & A. H. Bridle (San Francisco: ASP), 213
Foster, P. N., & Boss, A. P. 1996, ApJ, 468, 784
Giménez, A., & Clausen, J. V. 1994, A&A, 291, 795
Goodman, A. A., Bastien, P., Meyers, P. C., & Ménard, F. 1990, ApJ, 359, 363
Goodman, A. A., Crutcher, R. M., Heiles, C., Myers, P. C., & Troland, T. H. 1989, ApJ, 338, L61
Gray, D. F. 1992, The Observation and Analysis of Stellar Photospheres (Cambridge: Cambridge Univ. Press)
Herbig, G. H. 1998, ApJ, 497, 736
Ivison, R. J., et al. 1998, ApJ, 494, 211
Jaschek, C., & Jaschek, M. 1987, The Classification of Stars (Cambridge: Cambridge Univ. Press)
Kalas, P., & Jewitt, D. 1997, Nature, 386, 52
Kuiper, T. B. H., Whiteoak, J. B., Fowler, J. W., & Rice, W. 1987, MNRAS, 227, 1013
Lada, E. A., & Lada, C. J. 1995, AJ, 109, 1682
Ladd, E. F., Lada, E. A., & Meyers, P. C. 1992, ApJ, 410, 168
Lamers, H. J. G. L. M., & Leitherer, C. 1993, ApJ, 412, 771
Millward, C. G., & Walker, G. A. H. 1985, ApJS, 57, 63
Pauls, T. 1999, BAAS, 194, 47.04
Pauls, T., & Schwartz, P. R. 1989, in The Physics and Chemistry of Interstellar Molecular Clouds, ed. G. Winnewisser & T. J. Armstrong (Berlin: Springer), 225
Peterson, D. M., & Scholz, M. 1971, ApJ, 163, 51
Preibisch, T. 1997, A&A, 324, 690
Preibisch, T., Zinnecker, H., & Herbig, G. H. 1996, A&A, 310, 456
Riley, J. M. 1989, MNRAS, 238, 1055
Schaller, G., Schaerer, D., Meynet, G., & Meader, A. 1992, A&AS, 96, 269
Schmidt-Kaler, T. H. 1982, in Landolt-Börnstein New Series, Vol. 2b (New York: Springer)
Straižys, V. 1992, Multicolor Stellar Photometry (Tucson: Pachart)
Tull, R. G., Macqueen, P. J., Sneden, C., & Lambert, D. L. 1995, PASP, 107, 251
Ungerechts, H., & Thaddeus, P. 1987, ApJS, 63, 645
van Dishoeck, E. F., & Black, J. H. 1982, ApJ, 258, 533
van Dishoeck, E. F., & de Zeeuw, T. 1984, MNRAS, 206, 338
Wannier, P. G., & Andersson, B.-G. 1996, in ASP Conf. Ser. 97, Polarimetry of the Interstellar Medium, ed. W. G. Roberger & D. C. B. Whittet (San Francisco: ASP), 522
Wannier, P. G., Moriarty-Schieven, G., Andersson, B.-G., Hilts, M., & Langer, W. D. 2000, in preparation
White, R. L. 1985, ApJ, 289, 698
Whittet, D. C. B. 1992, Dust in the Galactic Environment (Bristol: IoP)
Whittet, D. C. B., & van Breda, I. G. 1987, A&A, 66, 57